Geochemistry Geophysics Geosystems G3

Article
Volume 12, Number 10
20 October 2011
Q10014, doi:10.1029/2011GC003757
ISSN: 1525-2027

Published by AGU and the Geochemical Society

Compositional and thermal equilibration of particles, drops, and diapirs in geophysical flows

M. Ulvrová
Laboratoire de Géologie de Lyon, École Normale Supérieure de Lyon, 46, Allée d'Italie, F-69364 Lyon CEDEX 07, France (martina.ulvrova@ens-lyon.fr)

N. Coltice and Y. Ricard
Laboratoire de Géologie de Lyon, Université de Lyon 1, Bat Geode, 43 Boulevard du 11 Novembre 1918, F-69100 Villeurbanne, France (nicolas.coltice@univ-lyon1.fr; ricard@ens-lyon.fr)

S. Labrosse
Laboratoire de Géologie de Lyon, École Normale Supérieure de Lyon, 46, Allée d'Italie, F-69364 Lyon CEDEX 07, France (stephane.labrosse@ens-lyon.fr)

F. Dubuffet
Laboratoire de Géologie de Lyon, Université de Lyon 1, Bat Geode, 43 Boulevard du 11 Novembre 1918, F-69100 Villeurbanne, France (fabien.dubuffet@univ-lyon1.fr)

J. Velímský
Department of Geophysics, Faculty of Mathematics and Physics, Charles University, V Holešovičkách 2, 180 00 Prague 8, Czech Republic (velimsky@karel.troja.mff.cuni.cz)

O. Šrámek
Department of Physics, University of Colorado at Boulder, 390 UCB, Boulder, Colorado 80309-0390, USA (ondrej.sramek@colorado.edu)

[1] Core formation, crystal/melt separation, mingling of immiscible magmas, and diapirism are fundamental geological processes that involve differential motions driven by gravity. Diffusion modifies the composition or/and temperature of the considered phases while they travel. Solid particles, liquid drops and viscous diapirs equilibrate while sinking/rising through their surroundings with a time scale that depends on the physics of the flow and the material properties. In particular, the internal circulation within a liquid drop or a diapir favors the diffusive exchange at the interface. To evaluate time scales of chemical/thermal equilibration between a material falling/rising through a deformable medium, we propose analytical laws that can be used at multiple scales. They depend mostly on the non-dimensional Péclet and Reynolds numbers, and are consistent with numerical simulations. We show that equilibration between a particle, drop or diapir and its host needs to be considered in light of the flow structure complexity. It is of fundamental importance to identify the dynamic regime of the flow and take into account the role of the inner circulation within drops and diapirs, as well as inertia that reduces the thickness of boundary layers and enhances exchange through the interface. The scaling laws are applied to predict nickel equilibration between metals and silicates that occurs within 130 m of fall in about 4 minutes during the metal rain stage of the Earth's core formation. For a mafic blob (10 cm diameter) sinking into a felsic melt, trace element equilibration would occur over 4500 m and in about 3 years.

Components: 6500 words, 5 figures, 1 table.

Keywords: equilibration; fluid mechanics; magma; mixing; modeling; segregation.

Index Terms: 1009 Geochemistry: Geochemical modeling (3610, 8410); 1043 Geochemistry: Fluid and melt inclusion geochemistry; 8145 Tectonophysics: Physics of magma and magma bodies.

Received 15 June 2011; **Revised** 29 August 2011; **Accepted** 30 August 2011; **Published** 20 October 2011.

Ulvrová, M., N. Coltice, Y. Ricard, S. Labrosse, F. Dubuffet, J. Velímský, and O. Šrámek (2011), Compositional and thermal equilibration of particles, drops, and diapirs in geophysical flows, *Geochem. Geophys. Geosyst.*, *12*, Q10014, doi:10.1029/2011GC003757.

1. Introduction

[2] Bubbles and crystals travel through differentiating magmas; metal drops and diapirs fell through molten silicates during the formation of Earth's core [*Stevenson*, 1990; *Rubie et al.*, 2003; *Samuel and Tackley*, 2008; *Monteux et al.*, 2009]; and sometimes, coexistent immiscible magmas or metals separate to reach gravitational equilibrium [*Dawson and Hawthorne*, 1973; *Dasgupta et al.*, 2006, 2009; *Morard and Katsura*, 2010]. Differential motion driven by gravity is a prerequisite for planetary differentiation at all scales. While a phase travels through and deforms the other, chemical and thermal diffusion proceed towards thermodynamic equilibrium. Depending on material and flow dynamics, non-equilibrium fractionation could result from inefficient mass/heat transfer from one phase to the other during travel. In order to quantify the time scale of thermodynamic equilibration, it is necessary to model deformation of both phases and transport dynamics.

[3] A generic physical description of these differentiation mechanisms can be formulated by the rise/fall of chemically (or thermally) distinct particles, drops or diapirs through a viscously deforming medium. In this paper, the term particle refers to a small self-contained body significantly more viscous than the surroundings and possibly solid, while drop and diapir are defined by self-contained bodies as viscous or less viscous than the surroundings and possibly inviscid. A diapir is a large-scale body with approximate sphericity, and we use the term of drop for small-scale body, when surface tension controls the sphericity. The purpose of this paper is to review and propose analytical laws that describe the chemical/thermal equilibration of a traveling particle, drop or diapir, that can be used at multiple scales and applied to a variety of geological problems. This chemical equilibration is that of minor or trace elements, migrating across the surface of the traveling sphere, assuming that the major element mineralogies, inside and outside the sphere, do not change. We first draw attention to results that are often overlooked in the geoscience literature though acknowledged in engineering and mass/heat transfer communities. Indeed, the mass and heat transfer between a liquid drop/solid particle and a viscous surrounding medium has been described for various industrial purposes [*Clift et al.*, 1978]. We then extend their use and couple them to concentration models inside and around the spherical body. We propose scaling laws for the time of equilibration for 4 different regimes: a particle with and without inertia, a drop/diapir with and without inertia. Then, we propose times of chemical equilibration during core formation and silicate melt differentiation.

2. Models for the Equilibration of Rising/Falling Particles, Drops, and Diapirs

2.1. Chemical and Thermal Transfer From a Sphere

[4] We restrict ourselves to the study of an individual spherical particle, drop or diapir of radius R in steady-state motion with terminal velocity U_t. In the following, the subscript "o" denotes the properties outside the sphere and "i" inside the sphere. The viscosity ratio between the falling/rising body and its host liquid is $\mathcal{R}_\mu = \mu_i/\mu_o$ and we speak of "particles" when $\mathcal{R}_\mu = \mu_i/\mu_o \gg 1$ and "drops" or "diapirs" when $\mathcal{R}_\mu = \mu_i/\mu_o \lesssim 1$. All the notations and parameters can be found in Table 1.

[5] In order for the dispersed phase to keep its sphericity, the interfacial force has to exceed disrupting forces, i.e. the viscous force and inertia, that tend to deform the sphere. The smallest drops or diapirs coalesce (they are swept by larger spheres traveling faster), the largest deform, stretch and eventually break-up. For highly viscous flows, the capillary number $\mathrm{Ca} = \mu_o U_t/\gamma$ (γ is interfacial tension), being the ratio between the viscous stresses and the interfacial tension, reaches a critical value for break-up conditions that depends on

Table 1. Variables and Parameters of the Studied System Together With Expressions for the Proposed Equilibration Times τ

Parameter	Notation	Unit
Viscosity of the host liquid	μ_o	Pa s
Viscosity inside the sphere	μ_i	Pa s
Diffusivity of the host liquid	D_o	$m^2\ s^{-1}$
Diffusivity inside the sphere	D_i	$m^2\ s^{-1}$
Density of the host liquid	ρ_o	kg m^{-3}
Density of the sphere	ρ_i	kg m^{-3}
Radius of the sphere	R	m
Terminal velocity	U_t	m s^{-1}
Initial concentration within the sphere	c_0	mol m^{-3}
Concentration at infinity	c_∞	mol m^{-3}
Dimensionless Number	**Notation**	**Expression**
Viscosity ratio	$\mathcal{R}_\mu$	μ_i/μ_o
Diffusivity ratio	$\mathcal{R}_D$	D_i/D_o
Reynolds number	Re	$RU_t\rho_o/\mu_o$
Peclet number	Pe	RU_t/D_o
Schmidt number	Sc	$\mathrm{Pe/Re} = \mu_o/(\rho_o D_o)$
Sherwood number	Sh	$-\langle \nabla C_o^{surf}\rangle/\langle C_o^{surf}\rangle$
Regime		**Equilibrium Timescale**
Drop: low Re, low $\mathcal{R}_\mu$		$\tau = \frac{\mathrm{Pe}}{3}\left(\frac{K}{0.461\left(1+\mathcal{R}_\mu\right)^{-1/2}\mathrm{Pe}^{1/2}} + \frac{1}{10\,\mathcal{R}_D}\right)$
Drop: high Re, low $\mathcal{R}_\mu$		$\tau = \frac{\mathrm{Pe}}{3}\left(\frac{K}{0.79\,\mathrm{Pe}^{1/2}} + \frac{1}{10\,\mathcal{R}_D}\right)$
Particle: low Re, high $\mathcal{R}_\mu$		$\tau = \frac{\mathrm{Pe}}{3}\left(\frac{K}{0.64\,\mathrm{Pe}^{1/3}} + \frac{3}{\pi^2\mathcal{R}_D}\right)$
Particle: high Re, high $\mathcal{R}_\mu$		$\tau = \frac{\mathrm{Pe}}{3}\left(\frac{K}{0.6\,\mathrm{Pe}^{1/3}\mathrm{Re}^{1/6}} + \frac{3}{\pi^2\mathcal{R}_D}\right)$

the viscosity ratio $\mathcal{R}_\mu$ across the surface. This critical capillarity number Ca is about 0.1 for high viscosity ratios and larger for low viscosity ratios, for which the drop/diapir stretches and forms a slender shaped body difficult to fragment (see *Stone* [1994] for a review). For low viscosity flows, perturbations of the interface generate Rayleigh-Taylor and Kelvin-Helmoltz instabilities that ultimately break up the drops [*Kitscha and Kocamustafaogullari*, 1989]. This situation happens when the Weber number $\mathrm{We} = \rho_o U_t^2 R/\gamma$ (ρ_o is external density), which is the ratio between inertia and interfacial tension, reaches values around 10 [*Wierzba*, 1990].

[6] For a body sinking or rising through a viscous medium, two non-dimensional numbers control the dynamics of chemical equilibration of the traveling sphere with its surroundings: (1) the Reynolds number $\mathrm{Re} = RU_t\rho_o/\mu_o$ that describes the effect of inertia to viscous force and (2) the Péclet number $\mathrm{Pe} = RU_t/D_o$ that relates the diffusion time to the advection time in the host liquid, D standing for chemical diffusivity. As both Re and Pe include the terminal velocity, it may be confusing to use simultaneously the two numbers and we introduce their ratio, also called the Schmidt number $\mathrm{Sc} = \mathrm{Pe/Re} = \mu_o/(\rho_o D_o)$. When the spherical body and its host liquid have different physical properties, the ratios of internal to external diffusivities $\mathcal{R}_D = D_i/D_o$ and viscosities $\mathcal{R}_\mu = \mu_i/\mu_o$, have to be considered.

[7] Starting from non equilibrium initial conditions, the sphere and its surroundings tend to chemically equilibrate by microscopic diffusion and macroscopic stirring. The stirring, i.e., the advection of concentration by the flow, occurs outside and possibly inside the sphere, due to the circulation forced by the shear stress at the surface of the drop.

[8] We assume that the initial concentration c of some trace element outside the sphere is uniform and equal to c_∞ while the concentration inside the drop is equal to c_0. The dimensionless transport equation governing this process, assuming materials are incompressible, is written as

$$\frac{\partial C}{\partial t} = \nabla \cdot \left(\frac{\mathcal{D}}{\mathrm{Pe}}\nabla C - \mathbf{v}C\right), \tag{1}$$

where C stands for the normalized concentration of any minor element of interest, i.e., $C = (c - c_\infty)/(c_0 - c_\infty)$ and $\mathcal{D}$ for the dimensionless diffusion coefficient being 1 outside the drop and $\mathcal{R}_D = D_i/D_o$ inside. To scale the quantities back to numbers with dimensions, the dimensionless distance has to be multiplied by the radius of the sphere R, and the time by the advection time R/U_t. The initial non-dimensional concentrations are one inside and zero outside.

[9] The local chemical equilibrium implies that the concentration c_i^{surf} on the inner side of the sphere is controlled by thermodynamics to be Kc_o^{surf}, where K is the partition coefficient at the surface ($K = c_i^{surf}/c_o^{surf}$). The final equilibrium is reached when the outside concentration is homogeneous and equal to c_∞ and the inside concentration also homogeneous but equal to Kc_∞. The normalized concentration inside the sphere, C_i, evolves therefore from 1 to $(K-1)c_\infty/(c_0 - c_\infty)$.

[10] The chemical and thermal diffusion of a traveling sphere is the subject of numerous studies in the chemical/heat transfer literature [e.g., *Clift et al.*, 1978; *Levich*, 1962] that we can only briefly introduce here. Usually the mass transfer coefficient of the sphere is defined as the Sherwood number:

$$\mathrm{Sh} = -R\frac{\langle \nabla c_o^{surf}\rangle}{\langle c_o^{surf}\rangle - c_\infty} = -\frac{\langle \nabla C_o^{surf}\rangle}{\langle C_o^{surf}\rangle}, \qquad (2)$$

where $\langle c_o^{surf}\rangle$ and $\langle C_o^{surf}\rangle$, and $\langle \nabla c_o^{surf}\rangle$ and $\langle \nabla C_o^{surf}\rangle$ are the average concentrations at the surface of the sphere and average gradients of concentration normal to it, with and without dimensions. The minus sign in equation (2) insures the positivity of Sh. Notice also that although the gradient of concentration $\langle \nabla c_o^{surf}\rangle$ can have any sign, the normalized gradient $\langle \nabla C_o^{surf}\rangle$ is always negative. Because of the similarity of heat and diffusion equations, all the results on diffusion relating Schmidt and Sherwood numbers have thermal counterparts where the mass flux is equivalent to the Nusselt number $\mathrm{Nu} = -R\nabla T_{surf}/(T_{surf} - T_\infty)$, and the Schmidt number to the Prandtl number $\mathrm{Pr} = \mu_o/(\rho_o\kappa_o)$, where T is temperature and κ thermal diffusivity.

[11] A very large number of semi-empirical equations predicting Sh, can be found in the literature, based on experiments and physical analysis. However, simple boundary layer theories can be developed to quantitatively describe mass fluxes at the interface in the different flow regimes. The general method is to express the velocity at the surface of the sphere, estimate the shape of the diffusion layer and perform careful averaging over the sphere [*Levich*, 1962; *Ribe*, 2007]. The general results for high enough Pe can be written in the form

$$\mathrm{Sh} = a\,\mathrm{Sc}^m\mathrm{Pe}^n = a\,\mathrm{Sc}^{m+n}\mathrm{Re}^n, \qquad (3)$$

where a, m and n are constants for a given regime. The exponents can be found by scaling arguments as summarized hereafter and the prefactor estimated analytically, numerically or experimentally:

[12] 1. When $\mathcal{R}_\mu \lesssim 1$, i.e., in the case where the internal viscosity is of the same order or smaller than the external viscosity, the external flow experiences the surface of the drop/diapir as a free-slip boundary condition. The surface velocity in the reference frame of the drop/diapir is therefore of order U_t, the transport term of the advection-diffusion equation $v.\nabla C$ is of order U_tC/R (transport along the surface of the sphere) and is balanced by a diffusion term $D_o\nabla^2 C$ of order D_oC/δ^2 across a diffusion boundary layer of thickness δ (diffusion perpendicular to the surface of the sphere). Therefore the diffusion boundary layer is of order $(\delta/R)^2 \propto 1/\mathrm{Pe}$, and, as $\mathrm{Sh} = R/\delta$

$$\mathrm{Sh} = a\,\mathrm{Pe}^{1/2} = a\,\mathrm{Sc}^{1/2}\mathrm{Re}^{1/2}. \qquad (4)$$

The details of the external velocity field control the diffusion layer and hence the expression of the constant a. (1) For low Re flows, inertia is negligible, the external velocity is given analytically by the Rybczynski-Hadamard expression [*Acrivos and Goddard*, 1965] and following *Levich* [1962] we obtain

$$a = 0.461\sqrt{\frac{1}{1+\mathcal{R}_\mu}}. \qquad (5)$$

(2) At very large Re, the flow becomes irrotational and the analytical expression of the potential flow yields $a = 0.79$ [*Clift et al.*, 1978].

[13] 2. When $\mathcal{R}_\mu \gg 1$, the sphere behaves rigidly. In its own reference frame, the surface velocity is zero then increases away to U_t. Two cases must then be considered. First, at low Re, there is no viscous boundary layer as viscous forces dominate everywhere in the domain. As a consequence the velocity increases from 0 to U_t over the distance R so that the velocity is of order $U_t\delta/R$ at the distance δ. The balance between advection and diffusion now gives $(U_t\delta/R)(C/R) \propto D_oC/\delta^2$, which leads to $(\delta/R)^3 \propto 1/\mathrm{Pe}$ and thus to

$$\mathrm{Sh} = a\,\mathrm{Pe}^{1/3} = a\,\mathrm{Sc}^{1/3}\mathrm{Re}^{1/3}, \qquad (6)$$

where $a = 0.64$ [*Levich*, 1962]. Second, at large Re, the situation is more complex. In this case, there is a viscous boundary layer of thickness δ' where the inertia term of the Navier-Stokes equation $\rho_o U_t^2/R$ is balanced by the viscosity $\mu_o U_t/\delta'^2$. The diffusive boundary layer is therefore embedded in a viscous layer of thickness $\delta' \propto R\ \mathrm{Re}^{-1/2}$. The velocity at the distance δ of the particle surface is of order $U_t\delta/\delta' = U_t\delta\mathrm{Re}^{1/2}/R$. The balance between diffusion and advection is now $(U_t\delta\mathrm{Re}^{1/2}/R)(C/R) \propto D_o C/\delta^2$ which leads to $(\delta/R)^3 \propto 1/(\mathrm{Re}^{1/2}\mathrm{Pe})$ and thus to

$$\mathrm{Sh} = a\,\mathrm{Re}^{1/6}\mathrm{Pe}^{1/3} = a\,\mathrm{Sc}^{-1/6}\mathrm{Pe}^{1/2} = a\,\mathrm{Sc}^{1/3}\mathrm{Re}^{1/2}, \quad (7)$$

where $a = 0.6$ [*Ranz and Marshall*, 1952].

[14] 3. For a non moving body, the diffusion equation can be solved exactly and Sh = 1. This is a special case, that does not obey the asymptotic equation (3) valid for high Pe. In the intermediate regime where Pe is small, various empirical expressions for each specific case can be found in the literature. For example, for $\mathrm{Re} \ll 1$, *Clift et al.* [1978] propose $\mathrm{Sh} = 1 + (1 + a^{4/3}\mathrm{Pe}^{2/3})^{3/4}$ in the case $\mathcal{R}_\mu \lesssim 1$ (which generalizes equation (4)) and $\mathrm{Sh} = 1 + (1 + a^3\mathrm{Pe})^{1/3}$ in the case $\mathcal{R}_\mu \gg 1$ (which generalizes equation (6)). These expressions are cumbersome and the cases where diffusion dominates advection not very interesting physically. For numerical applications, the reader should use the maximum of the asymptotic equation (3) and of the diffusive limit Sh = 1.

2.2. Equilibration Time Scales

[15] Once the Sherwood number is known (the average concentration gradient), to compute the evolution of the concentration within the sphere, we must now relate $\langle C_o^{\mathrm{surf}}\rangle$ to $\langle C_i\rangle$, the average concentration of the spherical body. Hence we integrate the diffusion equation (1) to get

$$\frac{\partial\langle C_i\rangle}{\partial t} = \frac{3}{\mathrm{Pe}}\langle\boldsymbol{\nabla} C_o^{\mathrm{surf}}\rangle = -3\frac{\mathrm{Sh}}{\mathrm{Pe}}\langle C_o^{\mathrm{surf}}\rangle. \quad (8)$$

The thermodynamic equilibrium at the surface implies $c_i^{\mathrm{surf}} = K c_o^{\mathrm{surf}}$, or in term of normalized concentrations,

$$C_i^{\mathrm{surf}} = K C_o^{\mathrm{surf}} + (K-1)\frac{c_\infty}{c_0 - c_\infty}. \quad (9)$$

[16] The concentration diffuses from the surface where the concentration gradient is $\langle\boldsymbol{\nabla} C_o^{\mathrm{surf}}\rangle/\mathcal{R}_D$. Therefore a reasonable profile for the radial concentration inside the drop is

$$C_i(r) = \langle C_i^{\mathrm{surf}}\rangle + \frac{\langle\boldsymbol{\nabla} C_o^{\mathrm{surf}}\rangle}{\mathcal{R}_D} f(r). \quad (10)$$

The function $f(r)$ characterizes the concentration profile and verifies the conditions at the surface and the center of the sphere: $f(1) = 0$, $f'(1) = 1$ and $f'(0) = 0$. This function should also satisfy some positivity constraint as the real concentration $c_i(r)$ should be everywhere positive. We do not impose such a condition. Our models implies that the concentration near the surface of the sphere is always positive and this controls the average concentration (related to the integral of $C_i(r)r^2$) which is always positive as we see below.

[17] Equation (10), averaged over the volume of the sphere, gives for the radial average concentration

$$\langle C_i\rangle = \langle C_i^{\mathrm{surf}}\rangle - \frac{\langle\boldsymbol{\nabla} C_o^{\mathrm{surf}}\rangle}{b\,\mathcal{R}_D} = \langle C_o^{\mathrm{surf}}\rangle\left(K + \frac{\mathrm{Sh}}{b\,\mathcal{R}_D}\right) + (K-1)\frac{c_\infty}{c_0 - c_\infty}, \quad (11)$$

where the second equality uses averaged equation (9), and where b is positive and given by

$$\frac{1}{b} = -3\int_0^1 f(r)r^2\mathrm{d}r. \quad (12)$$

[18] Combining equations (8) and (11) we predict an exponential homogenization of the concentration

$$\frac{\partial\langle C_i\rangle}{\partial t} = -\frac{1}{\tau}\left(\langle C_i\rangle - (K-1)\frac{c_\infty}{c_0 - c_\infty}\right) \quad \text{with} \quad \tau = \frac{\mathrm{Pe}}{3}\left(\frac{K}{\mathrm{Sh}} + \frac{1}{b\mathcal{R}_D}\right). \quad (13)$$

With real dimensions, the solution is simply

$$\langle c_i(t)\rangle = c_0\exp\left(-\frac{U_t}{R\tau}t\right) + Kc_\infty\left(1 - \exp\left(-\frac{U_t}{R\tau}t\right)\right). \quad (14)$$

These last expressions show that the average concentration in the sphere reaches exponentially the asymptotic equilibrium value and provides an estimate of the characteristic homogenization time τ as a function of K, Pe, Re, $\mathcal{R}_D$ and $\mathcal{R}_\mu$ (which controls the appropriate expression of Sh). It also shows that the average concentration is always positive, independently of the choice of $f(r)$, hence b, that we estimate for two limiting cases:

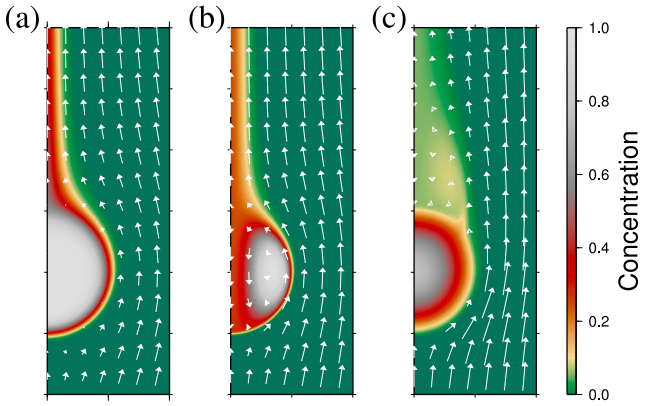

Figure 1. Maps (close-ups) of the nondimensional velocity relative to the average drop velocity (arrows) and concentration (color) for falling (a) particle in Re < 1 flow, (b) drop in Re < 1 flow (in to out viscosity ratio $\mathcal{R}_\mu = 10^{-3}$) and (c) particle in a higher Re flow (being 50 here). The spheres fall under their own weight and start with a composition of 1 (light grey) and the surrounding material has a zero concentration initially (green). All models have Péclet number Pe = 2800 and equal diffusivity in and out of the sphere ($\mathcal{R}_D = 1$). Snapshots are taken after a falling distance of 36 (Figure 1a), 41 (Figure 1b) and 283 (Figure 1c), times the sphere radius.

[19] 1. When $\mathcal{R}_\mu \gg 1$, there is no recirculation inside the sphere. When diffusivity of the outer material is large, $1/(b\mathcal{R}_D) \gg K/\mathrm{Sh}$, the time of equilibration in dimensional quantities is $\tau = R^2/(3bD_i)$, which is the same as the classical value obtained for diffusion in a sphere with imposed surface concentration $R^2/(\pi^2 D_i)$ [*Carslaw and Jaeger*, 1959], when $b = \pi^2/3$. This is obtained for $f(r) = -\sin(\pi r)/(\pi r)$, which indeed verifies $f'(0) = f(1) = 0$, and $f'(1) = 1$. In our equilibration experiments, the concentration is not imposed at the sphere surface but at infinity. The diffusion toward the sphere must also proceeds outside the sphere and using equation (13) with Sh = 1 we predict for the equilibration time of a static sphere (with real dimension)

$$\tau_s = K\frac{R^2}{3D_o} + \frac{R^2}{\pi^2 D_i}. \qquad (15)$$

The equilibration of a sphere with concentration maintained at infinity is indeed slower than when this concentration is imposed at the surface and depends on internal and external diffusivities and on the partition coefficient.

[20] 2. When $\mathcal{R}_\mu \lesssim 1$, there is an internal recirculation inside the drop/diapir, the concentration at the center is close to the concentration at the surface because of the efficient inner transport. Thus, the radial concentration profile within the fluid sphere must also satisfy $f(0) = 0$. The simplest polynomial function that verifies all four conditions $f(0) = f'(0) = f(1) = 0$, and $f'(1) = 1$ is $f(r) = r^2(r-1)$ which results in $b = 10$.

[21] For the convenience of the reader, the expressions for the equilibration times in the different regimes are summarized in Table 1.

3. Numerical Examples

[22] The goal of this section is to compare full numerical solutions for the time of equilibration with the analytical laws proposed above. Hence we run 2D axisymmetric numerical simulations of the incompressible Navier-Stokes equation coupled with the mass transfer equation. The experiments are performed using the finite element method (FEM) implemented in the Elmer open software (CSC IT–Center for Science, 2010, available at http://www.csc.fi/english/pages/elmer). The computing domain consists of an axisymmetrical cylinder with height and diameter of 40 R. In the center of the cylinder is a motionless sphere of radius R. Constant inflow of magnitude U_t parallel to the axis of symmetry together with zero concentration boundary condition are prescribed at the bottom of the cylinder, neglecting thus the influence of other drops. Free-slip boundary condition for velocity, and zero concentration are imposed at the sides of the cylinder. At the top, a flow parallel to the symmetry axis is forced, and a Neumann boundary condition of zero concentration gradient is prescribed. Finally, at the surface of the sphere, zero normal velocity and zero tangent traction are prescribed. A jump in concentration is imposed according to the choice of the partition coefficient, while the concentration flux remains continuous.

[23] Using FEM allows us to refine the mesh in the boundary layer around the sphere in order to have a good resolution for the velocity and transport equations, together with the refinement in the wake where more complicated structures of the flow appear at high Re. We use up to 80 000 mesh nodes. For each of the simulations, the time of equilibration τ is computed through a least-squares fit of the time series of $\langle C_i(t)\rangle$. We explore its dependence on the non-dimensional numbers Pe in the range 10^2–10^5, Re in the range 0–170 and diffusivity and viscosity ratios $\mathcal{R}_D$ and $\mathcal{R}_\mu$, in the range 10^{-1}–10^3 and 10^{-3}–10^3, respectively.

[24] Typical flows are shown in Figure 1 (velocity in the sphere reference frame is depicted by arrows, concentration by color scale). For a rigid sphere and low Reynolds number (panel a, $\mathcal{R}_\mu$ = 100, Re = 0.1), the flow is a typical Stokes flow, homogenization proceeds from the surface, and a tail is emitted in the wake of the sphere. When the internal viscosity is reduced keeping the same low Reynolds number (panel b, $\mathcal{R}_\mu = 10^{-3}$, Re = 0.1), a circulation is induced within the drop with velocities comparable to the terminal velocity, and we note two minima for the concentration, along the symmetry axis and at the surface. As Re increases (panel c, $\mathcal{R}_\mu = 10^4$, Re = 50), the symmetry of the flow breaks down and a vortex is generated behind the sphere. The variety of flows, within and outside the sphere, is the expression of the diversity of regimes for chemical and heat transfer. The transition from the drop/diapir case, in which the inner circulation is pronounced, and the particle case, where the sphere acts as a solid, occurs for $\mathcal{R}_\mu$ between 1 and 500 in our calculations.

[25] In Figure 2 we depict the average radial concentrations corresponding to cases with and without internal recirculation, for the situations and times of the cases in Figures 1b and 1c (the case in Figure 1a, without recirculation is comparable to the case in Figure 1c for what concerns the average radial concentration). Although the fits are not perfect, the analytical profiles capture the behavior of the numerical solutions. The quality of the approximations are increasing with time, as equilibration proceeds. As the average concentrations in the sphere involves $C_i(r)r^2$, and are therefore mostly controlled by the concentration near r = 1, more accurate fits are not needed.

[26] To benchmark the quality of the predictive laws proposed above, we compute the evolutions of the concentrations in numerical simulations. These evolutions can be closely matched by exponentials, as predicted. In Figure 3, the Pe dependence proposed above reproduces the results of the simulations in the various cases, at low and high Re. The proposed analytical expressions are in very good agreement with the numerical experiments. For the drop/diapir case, the analytical model with inviscid flow gives a lower bound for the time of equilibration since viscosity should slow motion in boundary layers. In Figure 3, the role of the circulation within the drop/diapir is expressed by the shorter equilibration time for the fluid sphere case relative to the solid case. Indeed, the circulation within the sphere produces efficient stirring that generates stronger chemical/thermal gradients which diffuse away more rapidly. As Pe increases, the non-dimensional time of equilibration increases. To keep the same reference time scale for the non-dimensionalization (fixing the values for U_t and R) while increasing Pe implies that diffusivity has to be decreased. It is then expected that keeping the velocity constant and decreasing the diffusivity thwarts equilibration.

[27] The observed role of Re in the simulations is also consistent with our predictions with and without internal circulation, as seen in Figure 4. Increasing Re leads to a decrease of the dimensionless time of equilibration. At high Re, velocities can be larger and stronger velocity gradients are allowed which favor a faster mixing. Indeed, the higher the Re the thinner the boundary layer around the sphere, and thus the more efficient the diffusion across the drop interface. However, this mechanism is somewhat modest since a limited reduction of the equilibration time by a factor of 2 requires more than 3 order of magnitude higher Re. The onset of the wake instability does not generate significant changes in the equilibration style mostly because the flux of elements/heat is dominated by the fluxes at the front of the sphere while it remains close to zero in the wake.

[28] Figure 5 shows τ as a function of $\mathcal{R}_D$ for a fixed Pe for the drop/diapir and particle cases at low and high Re. Again the numerical results show a good agreement with our theoretical predictions: when $\mathcal{R}_D > 1$, diffusion inside the sphere is more efficient than outside. Hence, diffusion in the host liquid is the limiting parameter for equilibration and τ does not depend on $\mathcal{R}_D$, cf. equation (13). For $\mathcal{R}_D < 1$, diffusion in the sphere is the limiting parameter and as a consequence τ decreases with $\mathcal{R}_D$. As explained above, the analytical model for the

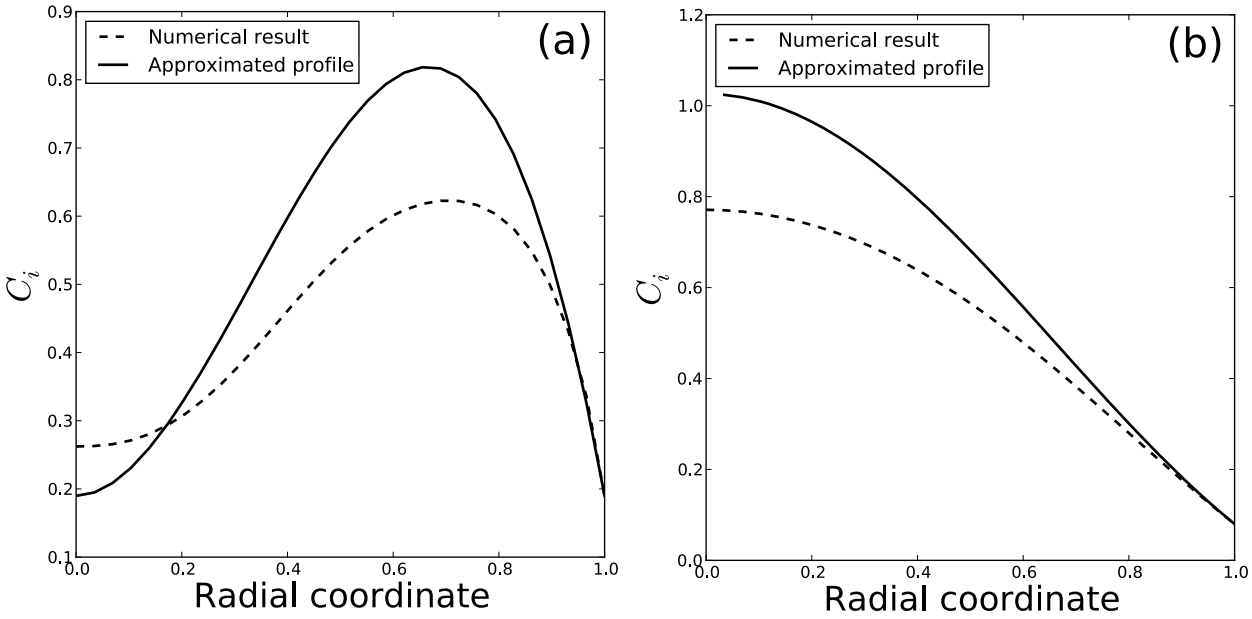

Figure 2. Average concentrations in the sphere as a function of normalized radius, corresponding to the cases in Figures 1b and 1c (solid lines). The profile approximations (dashed lines), equation (10) with $f(r) = r^2(r - 1)$ and $f(r) = -\sin(\pi r)/(\pi r)$, are in reasonable agreement with the simulations, particularly near $r = 1$.

high Re drop regime represents a lower bound for the analytical model since inviscid fluid is considered.

4. Discussion and Conclusions

[29] We presented approximate analytical models to predict equilibration times for spherical particles, drops and diapirs traveling through a viscously deforming surroundings due to buoyancy forces. Numerical simulations for a wide range of parameters confirm our predictive laws that can be used in geophysical problems at any scale. Small differences between analytical and numerical predictions can however be noticed (particularly visible in Figure 4 where we use a vertical linear scale). This might be due to the several assumptions of the analytical models (asymptotic expressions and choices of simple radial profiles) or of the numerical simulations (finite size of the computation domain).

[30] We showed that it is fundamental to take into account the flow structure and hence evaluate the correct regime for a given situation. The existence of an internal circulation within the spherical body is essential since it significantly reduces the time needed for equilibration. Compared to the purely diffusive systems, advective motion gives rise to thinner boundary layers and thus raises concentration gradients. Consequently, diffusion transport inside the spherical body and whole equilibration are more efficient than for a particle or motionless drop/diapir. When inertia dominates over the viscous forces, the boundary layer is even thinner speeding up further diffusion across the rim. Concerning the role of diffusivity and viscosity, a high diffusion rate of the surrounding host liquid always favors a rapid equilibration. The role of the external viscosity is more complex. The time of equilibration decreases both when the external viscosity is too low (in which case no stirring occurs within the drop) and when it is too large (in which case the terminal velocity and the internal velocities also decrease). The cases where the internal and external viscosities are close, i.e., the transition between drops (internal recirculation) and particles (no internal recirculation), are difficult to predict analytically. In the low Re number limit, the flow can be expressed as a function of $\mathcal{R}_\mu$ by the Rybczynski-Hadamard formulae but a choice has to be made for the value of b ($b = 10$ for a drop, $b = \pi^2/3$ for a particle). The situation is even more complex at high Re numbers where the real solution lies in between the two analytical cases.

[31] The predictive laws are scale-independent and can be applied to various geophysical settings without computing the full mass transfer problems. A small scale problem is hybridization of mafic blob falling in a more silicic melt. We choose typical numbers as those of *Grasset and Albarède* [1994]: 200 kg m^{-3} density excess than the felsic surroundings [*Huppert et al.*, 1982], viscosities of 500 Pa s

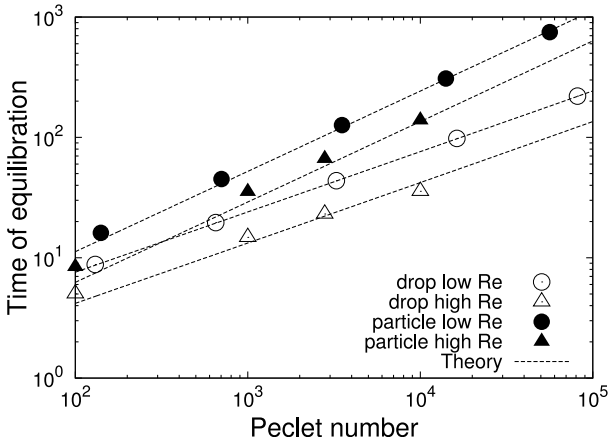

Figure 3. Nondimensional time of equilibration as a function of Péclet number (Pe) for drops and particles, at Re = 0 and Re = 50. In these simulations, the ratio of internal to external diffusivity is $\mathcal{R}_D = 1000$ and for the drop $\mathcal{R}_\mu = 0.1$. The analytical relationships are depicted by dashed lines.

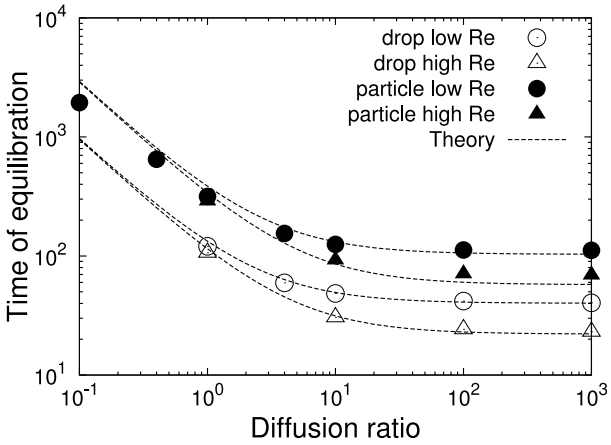

Figure 5. Nondimensional equilibration time as a function of diffusivity ratio $\mathcal{R}_D$ for drops and particles, at low and higher Reynolds number Re (Re = 0 and 50 here). In these simulations the Péclet number is Pe = 2800 and for the drop viscosity ratio $\mathcal{R}_\mu = 0.1$. The analytical relationships are depicted by dashed lines.

and 25000 Pa s for the mafic blob and host silicic melt and viscosity, respectively, and 10 cm for the blob diameter. The Rybczynski-Hadamard formula gives a terminal velocity of $U_t = 5.3 \cdot 10^{-5}$ m s^{-1} which implies Re = $2 \cdot 10^{-7}$. The corresponding dynamic regime is that of a drop traveling at low Re. To compute the time of equilibration we use typical

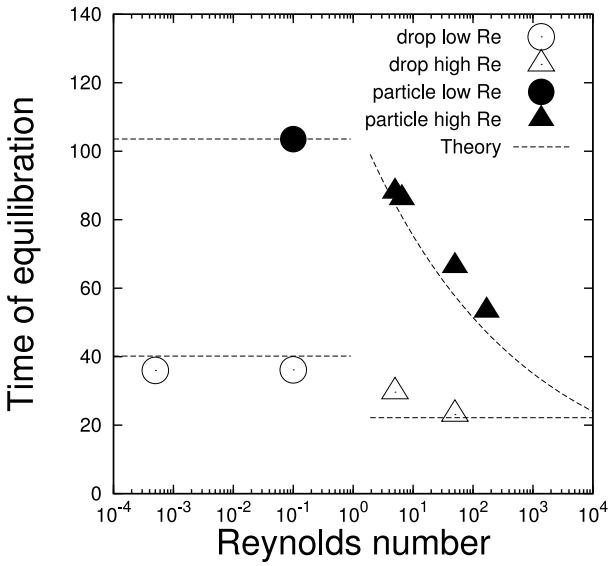

Figure 4. Nondimensional time of equilibration as a function of Re for drops and particles. In these simulations the Péclet number is Pe = 2800, ratio of internal to external diffusivity is $\mathcal{R}_D = 1000$ and for the drop case, ratio of in and out viscosities is $\mathcal{R}_\mu = 0.1$. The analytical relationships for low and high Re are depicted by dashed lines. The transition from low to high Re regime happens around Re = 1.

diffusion coefficients of 10^{-12} m^2 s^{-1} for trace elements for both liquids. As a consequence, Pe is about $2.7 \cdot 10^6$. We arbitrarily choose a partition coefficient of 2 between the two melts which means that a trace element will be twice more abundant in the mafic enclave than in the silicic melt after full equilibration. The mafic blob is much less viscous than the surrounding melt. Stirring inside the body thus enhances the hybridization rate and the characteristic time of equilibration is 2.7 years corresponding to a falling distance of 4535 m. This is a significantly shorter time than if equilibration proceeded only by static diffusion obtained from equation (15). Without any movement the equilibration could be attained in about 60 years. Notice, that many people would use the classical expression $\tau = R^2/(\pi^2 D_i)$ that gives for this case an equilibration time of 8 years, but is physically inappropriate as it neglects the diffusion in the surroundings of the sphere and the partition coefficient.

[32] For small iron droplets falling through a silicate magma ocean during early planetary differentiation, we use values similar to those given by *Rubie et al.* [2003], with a drop size of $R = 0.5$ cm. The most uncertain and critical parameter is the viscosity of molten silicates composing the magma ocean ranging in a wide interval 10^{-4}–100 Pa s. Choosing 0.01 Pa s gives us a terminal velocity U_t = 0.6 m s^{-1} using the work of *Brown and Lawler* [2003] for high Re flows. The viscosity of iron droplets is fixed at $\mu_i = 0.01$ Pa s [*Vočadlo et al.*, 2000] and we choose a partition coefficient of $K = 30$, which would be that for nickel at a pres-

sure of 50 GPa [*Li and Agee*, 2001]. The diffusivity of nickel in liquid iron is set to $D_i = 10^{-8}$ m^2 s^{-1} which is estimated from self-diffusion in liquid Fe at high pressure [*Dobson*, 2002]. The diffusion coefficient in molten silicate is chosen to be $D_o = 10^{-9}$ m^2 s^{-1}, imposing a diffusion ratio of 10. Using parameters above results in Pe, Re, and $\mathcal{R}_\mu$ of 3×10^6, 1000, and 1, respectively. Hence, the regime is that of a drop in a high Re fluid. In this case equilibration should be attained in 4 minutes with a traveled distance around 126 m. This distance is certainly shorter than the depth of a magma ocean that could be generated from an impact with a Mars-sized object [*Tonks and Melosh*, 1992]. Our predictions are of the same order of magnitude as the results obtained by *Rubie et al.* [2003] considering the uncertainties on the parameters. However, our theory takes into account the flow within the drop and effect of high Re, and thus proposes an intrinsically faster time of equilibration and shorter distance than *Rubie et al.* [2003].

[33] Further applications can be made (crystal settling in granitoids or ignimbrites, immiscible silicate and carbonatitic melts segregation etc…) using the correct proposed predictive relationships. However, we have made 3 main assumptions that have to be considered as limitations:

[34] 1. First, sphericity was assumed, which is known to be matched for drops when the surface tension dominates and for low Re, and for solids having a spheroidal shape. The deformation of diapirs and drops by viscous stresses along the boundaries can lead to peculiar shapes possibly skirted and with instabilities leading to break-up. More complex calculations have to be performed to follow the shape evolution in such case.

[35] 2. A second assumption involves non-interacting bodies. In the case of the previously advocated metallic rain in magma oceans the coalescence and influence of neighboring droplets have to be taken into account [*Ichikawa et al.*, 2010].

[36] 3. Third, we assumed pure buoyancy driven flow. The settling of particles and drops can be influenced by the effect of rotation or other forces that we have not considered in the present study.

Acknowledgments

[37] This work has been supported by the Agence Nationale de la Recherche under grant ANR-08-JCJC-0084-01 (Dyn-BMO). J.V. acknowledges the support of the Grant Agency of the Czech Republic, project P210/11/1366. Numerical models where performed using the free FEM software Elmer, from CSC. This paper also benefited from LaTeX, GMT and Gnuplot magic. We thank J. Rudge and P. J. Tackley for constructive reviews.

References

Acrivos, A., and J. Goddard (1965), Asymptotic expansions for laminar forced-convection heat and mass transfer, *J. Fluid Mech.*, *23*, 273–291.

Brown, P. P., and D. Lawler (2003), Sphere drag and settling velocity revisited, *J. Environ. Eng.*, *129*, 222–231.

Carslaw, H. S., and J. C. Jaeger (1959), *Conduction of Heat in Solids*, Clarendon, Oxford, U. K.

Clift, R., J. R. Grace, and M. Weber (1978), *Bubbles, Drops, and Particles*, Academic, New York.

Dasgupta, R., M. Hirschmann, and K. Stalker (2006), Immiscible transition from carbonate-rich to silicate-rich melts in the 3 GPa melting interval of eclogite plus CO_2 and genesis of silica-undersaturated ocean island lavas, *J. Petrol.*, *47*, 647–671.

Dasgupta, R., A. Buono, G. Whelan, and D. Walker (2009), High-pressure melting relations in Fe-C-S systems: Implications for formation, evolution, and structure of metallic cores in planetary bodies, *Geochim. Cosmochim. Acta*, *73*(21), 6678–6691.

Dawson, J., and J. Hawthorne (1973), Magmatic sedimentation and carbonatitic differentiation in kimberlite sills at Benfontein, South Africa, *J. Geol. Soc. London*, *129*, 61–85.

Dobson, D. (2002), Self-diffusion in liquid Fe at high pressure, *Phys. Earth Planet. Inter.*, *130*, 271–284.

Grasset, O., and F. Albarède (1994), Hybridization of mingling magmas with different densities, *Earth Planet. Sci. Lett.*, *121*(3–4), 327–332.

Huppert, H., J. Turner, and R. Sparks (1982), Replenished magma chambers—Effects of compositional zonation and input rates, *Earth Planet. Sci. Lett.*, *57*(2), 345–357.

Ichikawa, H., S. Labrosse, and K. Kurita (2010), Direct numerical simulation of an iron rain in the magma ocean, *J. Geophys. Res.*, *115*, B01404, doi:10.1029/2009JB006427.

Kitscha, J., and G. Kocamustafaogullari (1989), Breakup criteria for fluid particles, *Int. J. Multiphase Flow*, *15*(4), 573–588.

Levich, V. (1962), *Physicochemical Hydrodynamics*, Prentice-Hall, Englewood Cliffs, N. J.

Li, J., and C. Agee (2001), The effect of pressure, temperature, oxygen fugacity and composition on partitioning of nickel and cobalt between liquid Fe-Ni-S alloy and liquid silicate: Implications for the Earth's core formation, *Geochim. Cosmochim. Acta*, *65*, 1821–1832.

Monteux, J., Y. Ricard, N. Coltice, F. Dubuffet, and M. Ulvrova (2009), A model of metal-silicate separation on growing planets, *Earth Planet. Sci. Lett.*, *287*(3–4), 353–362.

Morard, G., and T. Katsura (2010), Pressure-temperature cartography of Fe-S-Si immiscible system, *Geochim. Cosmochim. Acta*, *74*, 3659–3667.

Ranz, W., and W. Marshall (1952), Evaporation from drops. 1, *Chem. Eng. Prog.*, *48*(3), 141–146.

Ribe, N. (2007), Analytical approaches to mantle dynamics, in *Treatise on Geophysics*, edited by G. Schubert, pp. 167–226, Elsevier, Amsterdam, doi:10.1016/B978-044452748-6.00117-6.

Rubie, D., H. Melosh, J. Reid, C. Liebske, and K. Righter (2003), Mechanisms of metal-silicate equilibration in the terrestrial magma ocean, *Earth Planet. Sci. Lett.*, *205*, 239–255.

Samuel, H., and P. J. Tackley (2008), Dynamics of core formation and equilibration by negative diapirism, *Geochem. Geophys. Geosyst.*, *9*, Q06011, doi:10.1029/2007GC001896.

Stevenson, D. (1990), Fluid dynamics of core formation, in *Origin of the Earth*, edited by H. E. Newsom and J. H. Jones, pp. 231–249, Oxford Univ. Press, New York.

Stone, H. (1994), Dynamics of drop deformation and breakup in viscous fluids, *Annu. Rev. Fluid Mech.*, *26*, 65–102.

Tonks, W., and H. Melosh (1992), Core formation by giant impacts, *Icarus*, *100*(2), 326–346.

Vočadlo, L., J. Brodholt, D. Alfe, M. Gillan, and G. Price (2000), Ab initio free energy calculations on the polymorphs of iron at core conditions, *Phys. Earth Planet. Inter.*, *117*, 123–137.

Wierzba, A. (1990), Deformation and breakup of liquid-drops in a gas-stream at nearly critical Weber numbers, *Exp. Fluids*, *9*(1–2), 59–64.